Combined Estimation of Cross-Sectional Area, Flow Rate and Pulse Wave Velocity Using Physics-Informed Neural Networks with 1D Hemodynamic Model Data

Javier Orera[1], Pilar García-Navarro[1], Javier Murillo[1], Julia Ramírez[1,2,3]

[1] Aragon Institute of Engineering Research, University of Zaragoza, Zaragoza, Spain
[2] Centro de Investigación Biomédica en Red, Biomateriales, Bioingeniería y Nanomedicina, Spain
[3] William Harvey Research Institute, Queen Mary University of London, London, United Kingdom

Abstract

The characterization of blood flow dynamics inside human vessels is essential for the personalised prediction and monitoring of cardiovascular risk. Accuracy is limited by the difficulty in the estimation of parameters of clinical relevance such as the Pulse Wave Velocity (PWV) and the evolution of the cross-sectional area and flow rate waves. In this work, we use Physics-Informed Neural Networks (PINNs) to simultaneously predict the propagation of non-linear waves inside arterial vessels as well as to estimate the PWV, in combination with a cost-effective PINN-based one-dimensional (1D) blood flow model. When departing from in-silico data derived from a 1D hemodynamic model, results reveal that highly precise estimates of the PWV (errors of $4\% \pm 2.5\%$) and accurate cross-sectional area and flow rate wave propagation predictions (errors of $\pm 2\%$) can be obtained by training the algorithm with blood flow velocity data pertaining exclusively to one virtual single sensor, showing the potential relevance of PINNs in the prediction of inverse problems in cardiovascular systems.

1. Introduction

Vascular aging is considered to be a measure of clinical interest. Aortic pulse wave velocity (PWV) is an hemodynamic index used to measure aortic stiffness that has been found to be an independent predictor of cardiovascular events and all-cause mortality [1].

Recent advances in computational vascular modelling endorse the use of numerical methods for the description of blood flow in whole-body close circulatory system, following a 1D approach. These 1D models [2] offer an accurate representation of hemodynamics, capturing the essential physics of blood circulation while remaining inexpensive and significantly faster than their three-dimensional counterparts.

Current research efforts aim to elucidate ways of bridging the gap between computational efficient and real-time in-the-loop applicability (digital twins), by putting forward customized 1D approaches that require a detailed description of the PWV in the different vessels [3] of the arterial tree.

In this work we make use of 1D predictive models in combination with PINNs to simultaneously: a) evaluate the prediction of the propagation of waves inside a blood vessel, as compared with an advanced numerical method, and b) infer the PWV inside the blood vessel from *in-silico* measurements in a very small data regime.

2. Methods

2.1. 1D Mathematical Models in blood vessels

1D blood flow models are used to represent the essential physical features of the propagation of pressure and flow waves in compliant vessels and consist of a system of two coupled Partial Differential Equations (PDEs) comprising the mass and momentum conservation equations:

$$\begin{aligned} \frac{\partial A}{\partial t} + \frac{\partial Q}{\partial x} &= 0 \\ \frac{\partial Q}{\partial t} + \frac{\partial}{\partial x}\left(\kappa \frac{Q^2}{A}\right) &= -\frac{A}{\rho}\frac{\partial p}{\partial x} \end{aligned} \tag{1}$$

where t is the time, x is the axial coordinate along the vessel, $A(x,t)$ is the local cross-sectional area, $Q = Au$ is the volume flow rate with $u(x,t)$ the cross sectional average velocity in the axial direction, $p(x,t)$ is the average internal pressure over the cross section expressing the response of the vessel wall deformation to pressure variations (see Figure 1a). The blood density is referred to as ρ, and a blunt velocity profile is assumed in this work by using $\kappa = 1$.

This system of equations is closed with a pressure-area relation of the form

 ISSN: 2325-887X DOI: 10.22489/CinC.2024.378

$$p(x,t) - p_e(x,t) = p_{tr}, \tag{2}$$

where p_e is the external pressure, and p_{tr} is the elastic transmural pressure. For the sake of simplicity, we will consider $p_e(x,t) = 0$, hence $p(x,t) = p_{tr}$. The elastic transmural pressure depends on the vessel stiffness K_0, the diastolic area $A_0 = A_0(x)$ and the reference pressure $p_0 = p_0(x)$. It is assumed of the form

$$p_{tr} = K_0\sigma + p_0, \quad \sigma = \left(\frac{A}{A_0}\right)^m - \left(\frac{A}{A_0}\right)^n = a^m - a^n, \tag{3}$$

with $a = A/A_0$ and σ the dimensionless transmural pressure difference. Transmural pressure for arteries is defined setting $m = 1/2$ and $n = 0$.

The vessel stiffness is related to the PWV as:

$$\text{PWV} = \sqrt{\frac{K_0}{\rho}(m-n)} \tag{4}$$

These equations can be nondimensionalized by choosing $a' = \frac{A}{A_0}$, $x' = \frac{x}{L}$, $t' = \frac{t}{T}$, $U = \frac{L}{T}$, $q' = \frac{Q}{A_0 U}$, $k' = \frac{K_0}{K}$, with L the length of the vessel and T a characteristic time.

$$\begin{aligned} \frac{\partial a'}{\partial t'} + \frac{\partial q'}{\partial x'} &= 0 \\ \frac{\partial q'}{\partial t'} + \frac{\partial}{\partial x'}\left(\frac{(q')^2}{a'}\right) &= -a'\frac{\partial p'}{\partial x'} \end{aligned} \tag{5}$$

The closure model is also nondimensionlized as:

$$p' = \frac{k' K\sigma}{\rho U^2} + \frac{p_0}{\rho U^2}, \quad \sigma = (a')^m - (a')^n, \tag{6}$$

Figure 1a depicts an isolated vessel, which will serve as case study throughout the remainder of this work. The model vessel is discretized into a number of cells, wherein the values of cross-sectional area (A), flow rate (Q) and pressure (p) are defined as piece-wise uniform variables.

2.2. Physics-Informed Neural Networks: Vanilla PINN

Physics-Informed Neural Networks incorporate the governing physical laws directly into the neural network architecture. The term *vanilla* PINN refers to the original algorithm as proposed in [4] for the integration of the PDEs into the neural network model.

Collocation points are points in space-time where the residual of the PDE is evaluated. By minimizing this residual at each collocation point, variables and its derivatives are driven towards the fulfillment of the PDE itself. Collocation points will be denoted with tuples (x_c, t_c) for the remainder.

For the system of PDEs described in Equation 1, the loss function of the vanilla PINN has the following form:

$$\boldsymbol{L} = \boldsymbol{L}_{PDE}^{vanilla} + \boldsymbol{L}_{data} \tag{7}$$

with:

$$\begin{aligned} \boldsymbol{L}_{PDE}^{vanilla} &= l_1 \tfrac{1}{n_c}\textstyle\sum_{c=1}^{n_c} \left(\frac{\partial a'}{\partial t'} + \frac{\partial q'}{\partial x'}\right)^2 \Big|_{(x'_c,t'_c)} \\ &+ l_2 \tfrac{1}{n_c}\textstyle\sum_{c=1}^{n_c} \left(\frac{\partial q'}{\partial t'} + \frac{\partial}{\partial x'}\left(\frac{q'^2}{a'}\right) + a'\frac{\partial p'}{\partial x'}\right)^2 \Big|_{(x'_c,t'_c)} \end{aligned} \tag{8}$$

$$\begin{aligned} \boldsymbol{L}_{data} = & \, l_3 \tfrac{1}{n_i}\textstyle\sum_{i=1}^{n_i} \left(q'(x',0) - q'_i(x',0)\right)^2 \\ & + l_4 \tfrac{1}{n_b}\textstyle\sum_{i=1}^{n_b} \left(q'(x'_b,t'_b) - q'_b(x'_b,t'_b)\right)^2 \\ & + l_5 \tfrac{1}{n_i}\textstyle\sum_{i=1}^{n_i} \left(a'(x',0) - a'_i(x',0)\right)^2 \\ & + l_6 \tfrac{1}{n_b}\textstyle\sum_{i=1}^{n_b} \left(a'(x'_b,t'_b) - a'_b(x'_b,t'_b)\right)^2 \\ & + l_7 \tfrac{1}{n_d}\textstyle\sum_{i=1}^{n_i} \left(q'(x'_d,t'_d) - q'_d(x'_d,t'_d)\right)^2 \\ & + l_8 \tfrac{1}{n_d}\textstyle\sum_{i=1}^{n_d} \left(a'(x'_d,t'_d) - a'_d(x'_d,t'_d)\right)^2 \end{aligned} \tag{9}$$

where n_c is the number of sampled collocation points, $(q', a') = \boldsymbol{PINN}(x', t'; \boldsymbol{w}, k')$ with $\boldsymbol{w}$ comprising the weights and biases of the neural network, n_i is the number of initial value points $q'_i(x', 0)$ and $a'_i(x', t' = 0)$, n_b is the number of boundary value points $q'_b(x'_b, t' > 0)$ and $a'_b(x'_b, t > 0)$ where $\partial\Omega$ represents to the vessel's inlet and outlet boundaries, and n_d refers to the number of data points available in the domain, through observations, measurements or simulations, that is fed to the training. All derivatives are evaluated at the collocation points (x'_c, t'_c) using automatic differentiation. Parameters $l_1, ..., l_8$ are weighting coefficients that have to be tuned so as to balance the magnitudes of the PDE loss $\boldsymbol{L}_{PDE}$ (from now on *collocation loss*) and the data loss $\boldsymbol{L}_{data}$.

Figure 1b represents a training step of a vanilla PINN [4] computing the loss with automatic differentiation, for the inverse problem.

2.3. Experimental design

Throughout the remainder of the study, we use a first-order finite-volume Riemann solver [5] to compute the ground truth solution $A(x,t)$, $Q(x,t)$ and $p(x,t)$ inside an elastic artery (hence $m = 1/2, n = 0$), given a predefined value of the vessel stiffness $K_0 = K = 966.014 \frac{kg}{cms^2}$. Using Equation 4 we can calculate the value of PWV $= 674 \frac{cm}{s}$. It is important to notice that the real value of PWV will be completely unknown for the PINN, but necessarily given to the numerical method, hence PWV will be inferred based exclusively on initial, boundary and vessel midpoint data.

Both numerical method and PINN will be provided with the diastolic area $A_0 = \pi r_d^2$ with $r_d = 0.3$ cm and the

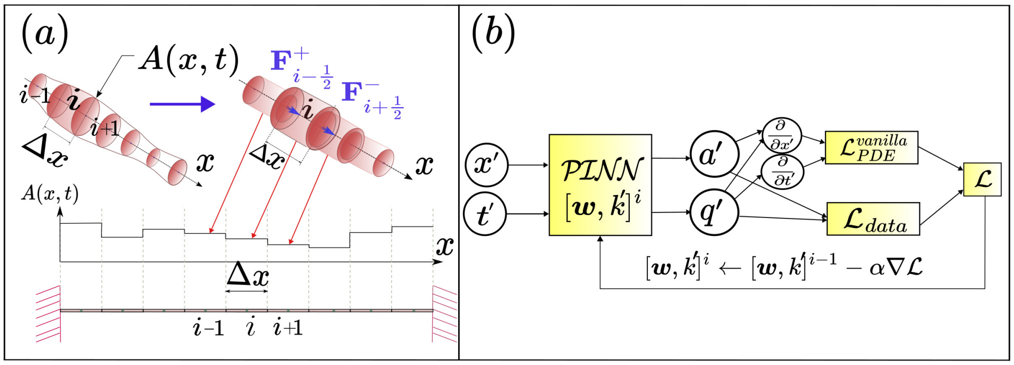

Figure 1. (a) Vessel discretization for the numerical method computation. (b) Chart-flow of inverse vanilla PINN using 1D vascular model.

average diastolic pressure $\hat{p_0} = 80.61$ mmHg. The length of the vessel will be $L = 12.6$ cm and the simulation time $T = 1s$.

As initial conditions at time $t' = 0$ and boundary conditions at inlet and outlet of the vessel, we consider the spatial and temporal profiles shown in Figures 2 and 3 for the cross-sectional area and flow rate, respectively.

Additionally, the evolution of the area and flow rate in the vessels midpoint are also depicted, as if we would place a virtual sensor at the vessel's midpoint. These latter are very important for the training process, since they are fed into the algorithm as data, hence the PINN is enforced to accurately reproduce these curves, and obtain accordingly a suitable value for PWV.

A total of 18 experiments where performed, varying the initial value of PWV to be 50%, 150% and 200% of its real value PWV $= 674\frac{cm}{s}$. In 15 of the 18 experiments midpoint data over time of cross-sectional area and flow rate were fed to the PINN. In the remaining 3 experiments only flow rate data over time at vessel midpoint was provided (initial and boundary conditions were always given as data), but no midpoint data of cross-sectional area was provided.

Regarding the neural network hyperparameter selection, a learning rate of $\alpha = 0.001$ was chosen for the Adam optimizer. The model architecture comprised 10 layers of 10 neurons each with activation function $tanh$.

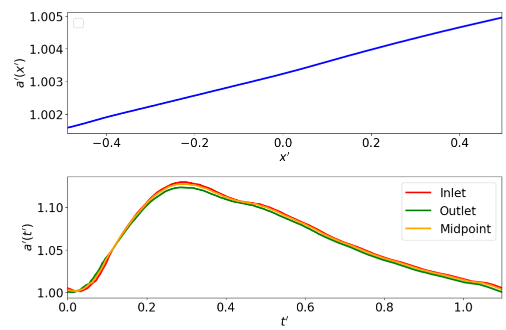

Figure 2. Cross-sectional area at $t' = 0$ (top) and cross-sectional area over time at vessel's inlet, midpoint and outlet (bottom).

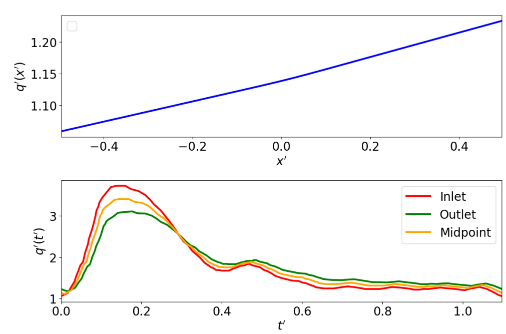

Figure 3. Flow rate at $t' = 0$ (top) and flow rate over time at vessel's inlet, midpoint and outlet (bottom).

3. Results

To quantify the uncertainty of the predictions of the PINN for the 18 experiments, we present the error margins around the predicted mean, calculated as $\mu + \sigma$ for the upper bound and $\mu - \sigma$ for the lower bound, where μ is the predicted mean and σ is the standard deviation of all the predictions.

We now track the evolution of the nondimensional stiffness k', which directly relates to the prediction of PWV. Figure 4 depicts the convergence of k' as the training process progresses. Initially, the value of k' is unstable but it gradually aligns more closely with the real value of the vessel's stiffness as iterations progress. Final predictions of PWV yielded a mean average error of $4\% \pm 2.5\%$.

Finally, PINN prediction errors of the propagation of cross-sectional area and flow rate waves are shown in Figures 5 and 6 respectively, using the predicted value of

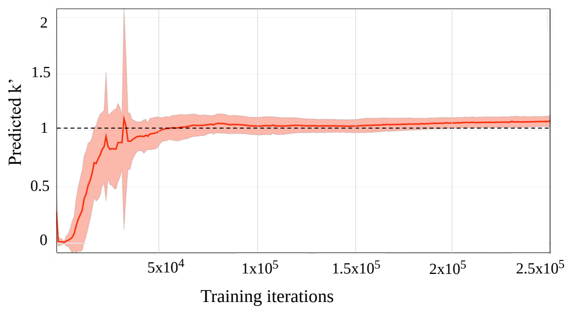

Figure 4. Evolution of the prediction of k' with training iterations.

PWV after PINN convergence. We observe very small errors for the prediction of the cross-sectional area at different points over time along the vessel ($\pm 0.3\%$) as well as for the flow rate ($\pm 2\%$), hence the predictions are very accurate and do not depend either on the initialization of the PWV nor the incorporation of midpoint data of the area.

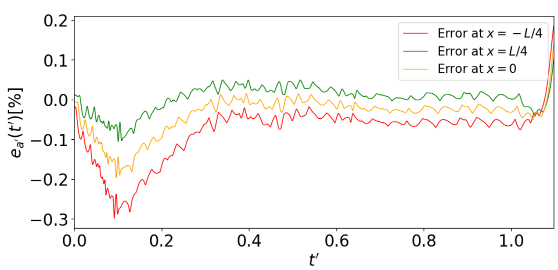

Figure 5. PINN prediction error of vessel's area at $x' = -L/4$, $x' = L/4$ and $x' = 0$.

4. Discussion and conclusions

The present study explores the use of PINNs to estimate PWV and cross-sectional area and flow rate wave propagation within human vessels using a 1D model of blood flow. This approach achieves high accuracy with minimal *in-silico* patient-specific data by training the PINN model with velocity data from a single virtual sensor affixed at the vessel's midpoint, as opposed to previous approaches that require prior knowledge on the PWV. In conclusion, we show that, in contrast to other predictive models that depend on extensive 3D flow simulations [6], effective non-invasive cardiovascular monitoring and diagnosis can be achieved even with very limited amounts of data. Future work will focus on more realistic scenarios where PWV varies along the vessel, and the application of our methodology to real clinical data.

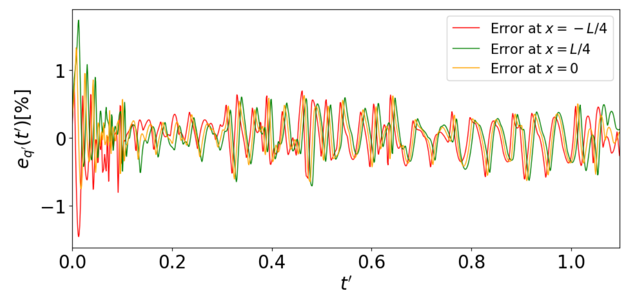

Figure 6. PINN prediction error of vessel's flow rate at $x' = -L/4$, $x' = L/4$ and $x' = 0$.

5. Acknowledgements

This work was supported by project 'IMPULSO' funded by the Aragon Institute of Engineering Research. JR acknowledges funding from grants PID2021-128972OA-100 and CNS2023-143599, and fellowship RYC2021-031413-I from Spanish Ministry of Science and Innovation.

References

[1] Hong J, Nandi M, Charlton PH, Alastruey J. Noninvasive hemodynamic indices of vascular aging: an in silico assessment. American Journal of Physiology Heart and Circulatory Physiology 2023;325(6):H1290–H1303.

[2] Murillo J, Navas-Montilla A, García-Navarro P. Formulation of exactly balanced solvers for blood flow in elastic vessels and their application to collapsed states. Comput Fluids 2019;186:74–98.

[3] Flores Gerónimo J, Keramat A, Alastruey J, Duan HF. Computational modelling and application of mechanical waves to detect arterial network anomalies: Diagnosis of common carotid stenosis. Computer Methods and Programs in Biomedicine 2022;227:107213. ISSN 0169-2607.

[4] Raissi M, Perdikaris P, Karniadakis GE. Physics-informed neural networks: A deep learning framework for solving forward and inverse problems involving nonlinear partial differential equations. J Comput Phys 2019;378:686–707.

[5] Murillo J, García-Navarro P. Weak solutions for partial differential equations with source terms: Application to the shallow water equations. J Comput Phys 2010; 229(11):4327–4368.

[6] Garay J, Dunstan J, Uribe S, Costabal FS. Physics-informed neural networks for blood flow inverse problems. arXiv preprint 2023;arXiv:2308.00927.

Address for correspondence:

Javier Orera

I3A, Universidad de Zaragoza, C/Mariano Esquillor s/n, 50018, Zaragoza, Spain

javier.orera@unizar.es